Journal of Inorganic and Organometallic Polymers and Materials (2024) 34:1272–1281
https://doi.org/10.1007/s10904-023-02899-z

RESEARCH

Preparation of Core-Shell Magnetic Microspheres and Its Application in Jasminaldehyde Condensation Reactions

Leiming Fu[1] · Qilin Diao[1] · Zhigeng Zhang[1] · Ruili Zhao[1] · Cun Li[1] · Linyan Yang[1]

Received: 6 September 2023 / Accepted: 5 October 2023 / Published online: 19 October 2023
© The Author(s), under exclusive licence to Springer Science+Business Media, LLC, part of Springer Nature 2023

Abstract

Metal nanoparticles (MNPs) have garnered significant attention due to their exceptional performance in heterogeneous reactions. Meanwhile, extensive applications have been found for metal-organic frameworks (MOFs), known for their ordered structure and high surface area. In this study, MNPs particles were amalgamated with MOFs to create a core-shell structure and were introduced amino groups into this configuration through post-synthetic modification (PSM), resulting in the successful synthesis of six distinct nanomaterials. Comprehensive characterization techniques, including infrared spectroscopy (IR), X-ray diffraction (XRD), and X-ray photoelectron spectroscopy (XPS), confirmed the synthesis and modification of the MNPs/MOFs materials. These synthesized materials were employed as catalysts for the condensation reaction of jasminaldehyde. It is noteworthy that these catalysts exhibited outstanding performance, showcasing advantages over traditional heterogeneous catalysts. This superior performance is attributed in part to the advanced core-shell structure of these materials and the effective introduction of amino functional groups through the PSM technique.

Keywords MOFs · MNPs · PSM · Jasminaldehyde condensation

1 Introduction

In recent decades, Metal Nanoparticles (MNPs) have drawn increasing attention as an essential class of nanocatalysts because of their superior activities in heterogeneous catalytic reactions in which the size of the MNPs is a significant factor in determining their performance [1]. Among them, maghemite(γ-Fe_2O_3) is widely used in different fields due to its ferromagnetic properties and chemical stability, such as catalysis [2], biomedicine [3], and drug delivery [4]. Metal-Organic Frameworks (MOFs) constitute a rapidly growing class of materials comprising metal ions or clusters as nodes and organic ligands as linkers [5]. Some applications of MOFs have been found in various fields, such as gas storage [6], liquid-phase separations and extractions [7], catalysis [8], and biomedicine [9]. MOFs have a large surface area, ordered configuration, multifunctional pore size, significant chemical stability, and high biological affinity for biomolecules. MIL-101-NH_2 is favored by researchers due to its hollow cage-like structure, excellent skeletal stability, and easier functionalization [10]. Therefore, MOFs can effectively accommodate many MNPs, confining their size, preventing migration, and forming stable core-shell structures [11]. The core-shell structure imbues them with enhanced catalytic activity and selectivity. The external shell offers active sites that facilitate the adsorption and reaction of catalytic substrates through surface interactions.

Additionally, the core nanoparticles, functioning as active catalyst centers, participate in synergistic interactions with the shell, further enhancing catalytic performance [12]. The core-shell configuration could also facilitate more efficient substrate diffusion and product release, minimizing catalyst poisoning and deactivation. This architecture enables catalytic substrates to experience enhanced diffusion between the core and shell, thereby optimizing reaction efficiency [13]. Research has shown that incorporating amino functional groups into MOFs could substantially augment the

✉ Ruili Zhao
zhaoruili1109@126.com

✉ Cun Li
hhlicun@163.com

✉ Linyan Yang
y_linyan@163.com

[1] Tianjin Key Laboratory of Agricultural Animal Breeding and Healthy Husbandry, College of Animal Science and Veterinary Medicine, Tianjin Agricultural University, Tianjin 300392, China

catalytic efficiency of alkaline catalysts [14]. The introduction of amino groups within the MOF structure could be achieved through Post-Synthetic Modification (PSM).

The catalytic condensation of benzaldehyde and 1-heptanal is a significant aldol-type reaction in producing a-pentyl cinnamaldehyde. The commercial name of this fine compound is jasminaldehyde, and most widely applied in the perfume industry. This aldol condensation is usually carried out in the presence of a homogeneous catalyst such as sodium or potassium hydroxide [15]. The main drawback of the homogeneous process for synthesizing jasminealdehyde is that the homogeneous catalyst cannot be reused and recycled [16]. In order to study the effect of the jasminealdehyde condensation reaction, a core-shell γ-Fe_2O_3/Al-MOF composite with a hierarchical porous structure was prepared by developing an Al-MOF around γ-Fe_2O_3 nanoparticles using one-pot synthesis, and six composite materials were prepared using PSM, as shown in Fig. 1. The catalytic activity in the supernatant was determined by gas chromatography-mass spectrometry.

2 Experimental Section

2.1 Materials and Physical Measurements

Sample γ-Fe_2O_3@SiO_2–NH_2-CMC (γ-Fe_2O_3-CMC) and γ-Fe_2O_3@SiO_2–NH_2-AA (γ-Fe_2O_3-AA) were synthesized according to the method reported previously [17]. Terephthalic acid (H_2BDC), 2-(N-morpholino) ethanesulfonic acid (MES), 1-(3-Dimethylaminopropyl)-3-ethylcarbodiimide hydrochloride (EDC), N-Hydroxysuccinimide (NHS), aspartic (Asp), glutamate (Glu) and glutaric anhydride (GA) were purchased from Shanghai Source Biological Technology Co., LTD (Shanghai, China). Adenine(A), ferric oxide(γ-Fe_2O_3), and aluminum chloride were purchased from Shanghai Macklin Biological Technology Co., LTD (Shanghai, China). 2-aminoterephthalic acid was purchased from RHAWN Reagent Co., LTD (Shanghai, China). All commercially available chemicals and solvents were of reagent grade and used without further purification. IR spectra were recorded in the range of 4000–400 cm^{-1} on a Perkin-Elmer spectrometer with KBr pellets. Changes in morphology and size could be characterized by Scanning Electronic Microscopy (SEM et al., China). X-ray powder diffraction (XRD) intensities were measured on a Rigaku D/max-IIIA diffractometer (Cu-Kα, λ = 1.54056 Å).

XPS spectra were recorded using a Kratos Axis Ultra DLD spectrometer employing a monochromated Al-Kα X-ray source (hv = 1486.6 eV). The vacuum in the main chamber was kept above 3×10^{-6} Pa during XPS data acquisitions. General survey scans (binding energy range: 0–1200 eV; pass energy: 160 eV) and high-resolution spectra (pass energy: 40 eV) in the regions of N1s and C1s were recorded. Binding energies were referenced to the C1s binding energy at 284.60 eV.

The catalytic data were obtained by GC-MS (Gas chromatography-mass spectrometry). The GC-MS system was from GCMS-TQ8040 (Shimadzu, Japan) GC-MS/MS triple quadrupole instrument equipped. Using fused-silica capillary columns: Rxi-5Sil MS (25 m × 0.25 mm i.d.,0.25 μm film thickness). The operational parameters for the GC–MS analysis were: carrier gas, helium; column temperature program 60 °C for 2 min, rising at 10 °C/min to 250 °C, then held for 2 min.

2.2 Preparation and Modifcation of MNPs/MOFs Particles

2.2.1 Preparation of MNPs/MOFs Particles

According to Li et al., using polysaccharide-modified MNPs materials as catalysts in the Knoevenagel reaction yields the highest conversion rate [18]. Therefore, two polysaccharides, sodium carboxymethyl cellulose (CMC) and sodium alginate (AA) were chosen to modify MNPs.

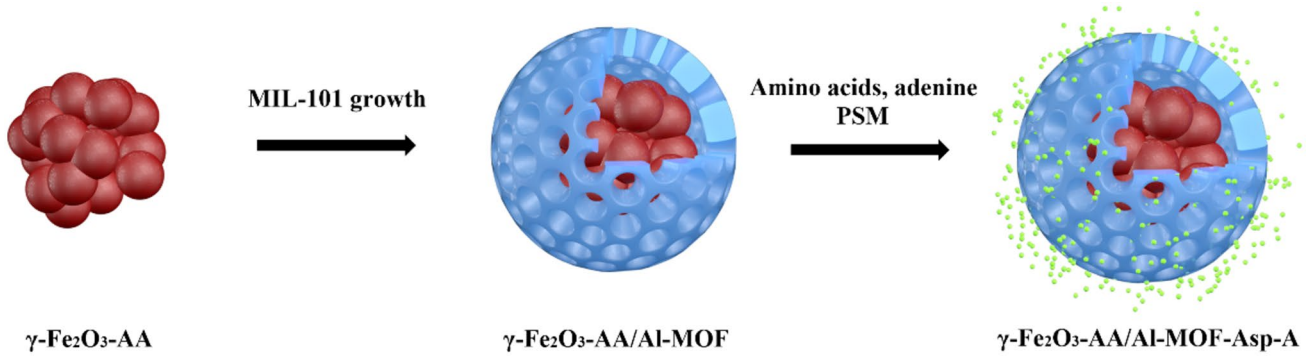

Fig. 1 Synthetic route

The γ-Fe_2O_3 MNPs were modified first with CMC and AA, which could be activated for binding via carboxyl functional groups [17]. Then, the carboxyl-modified γ-Fe_2O_3 MNPs were covered by Al-MOFs by a one-pot synthesis method with a core–shell structure. In detail, γ-Fe_2O_3 (10 mg) was acidified with HCl under 100 W of ultrasound for 20 min. Concentrated NH_3·–H_2O (250 mL) was added to the samples of γ-Fe_2O_3. TEOS (32 mL) was added to the samples, and the samples were then oscillated at 140 rpm for 6 h, and the residue was washed with ethanol twice to yield γ-Fe_2O_3@SiO_2 nanoparticles. APTMS (50 mL) was added dropwise to the sample of γ-Fe_2O_3@SiO_2 obtained previously, and the mixture was reacted for 24 h. After rinsing with ethanol twice, the γ-Fe_2O_3@SiO_2–NH_2 nanoparticles were dried under vacuum overnight. A CMC and AA solution was converted into N-hydroxysuccinimide esters by sequential reaction with EDC and NHS. The solution was finally introduced to freshly prepared γ-Fe_2O_3@SiO_2–NH_2 nanoparticles. After washing with ethanol, samples of γ-Fe_2O_3@SiO_2–NH_2–CMC and γ-Fe_2O_3@SiO_2–NH_2-AA could be obtained after drying under vacuum.

0.1 g of γ-Fe_2O_3@SiO_2–NH_2-CMC nanoparticles were added to a mixed solution of DMF (50 mL), 2-aminoterephthalic acid (0.992 g), and $AlCl_3$ (0.5 g). The resulting mixture was transferred to a three-necked flask and placed in an oil bath at 130 °C for 24 h with stirring to yield γ-Fe_2O_3@SiO_2–NH_2-CMC/MIL-101(Al)–NH_2 (γ-Fe_2O_3-CMC/Al-MOF) nanoparticles, and γ-Fe_2O_3@SiO_2–NH_2-AA/MIL-101(Al)–NH_2 (γ-Fe_2O_3-AA/Al-MOF) nanoparticles were fabricated in the same steps as above. Finally, the obtained two kinds of nanoparticles were washed several times with DMF and ethanol and then dried under vacuum at 100 °C overnight for further assay use.

2.2.2 Modifcation of MNPs/MOFs Particles

Three molecules containing two carboxyl functional groups, namely, aspartic (Asp), glutamate (Glu), and glutaric anhydride (GA), were selected to facilitate the bonding of adenine. The modification of MOFs with amino acids enhances alkaline sites and hydrothermal stability [19]. Adenine, serving as the source of Lewis basic sites, also augments the corresponding catalytic activity [20].

0.835 g of 2-(N-morpholino)ethanesulfonic acid (MES) and 1.169 g of NaCl were weighed and placed into 40 mL of ultrapure water. The pH of the MES buffer solution was adjusted to 6 using 0.1 mol/L NaOH. Glutamate powder at a concentration of 2 mg/mL was added and stirred to dissolve, resulting in a glutamate solution. Into the MES buffer solution, 1–2 equivalents of 1-(3-dimethylaminopropyl)-3-ethylcarbodiimide hydrochloride (EDC, 38.4 mg/mL) and N-hydroxysuccinimide (NHS, 38.4 mg/mL) were placed. The amino acids were activated using ultrasonic for 1 h. The prepared amino acid solution was combined with γ-Fe_2O_3-CMC/Al-MOF powder (0.5 g/40 mL) and transferred to a 50 mL centrifuge tube. The tube was sealed with a sealing film and placed on a shaker at room temperature with a rotation speed of 140 rpm for 78 h. Bubbles generated during the reaction were removed, the mixture was centrifuged, and the supernatant was discarded. After two washes with anhydrous ethanol, the sample was dried in a vacuum drying oven at 80 °C for 24 h, yielding powdered samples of γ-Fe_2O_3@SiO_2–NH_2-CMC/MIL-101(Al)–NH_2-Glu (γ-Fe_2O_3-CMC/Al-MOF-Glu), γ-Fe_2O_3@SiO_2–NH_2-CMC/MIL-101(Al)–NH_2-Asp (γ-Fe_2O_3-CMC/Al-MOF-Asp), γ-Fe_2O_3@SiO_2–NH_2-CMC/MIL-101(Al)–NH_2-GA (γ-Fe_2O_3-CMC/Al-MOF-GA), γ-Fe_2O_3@SiO_2–NH_2-AA/MIL-101(Al)–NH_2-Glu (γ-Fe_2O_3-AA/Al-MOF-Glu), γ-Fe_2O_3@SiO_2–NH_2-AA/MIL-101(Al)–NH_2-Asp (γ-Fe_2O_3-AA/Al-MOF-Asp) and γ-Fe_2O_3@SiO_2–NH_2-AA/MIL-101(Al)–NH_2-GA (γ-Fe_2O_3-AA/Al-MOF-GA) for subsequent testing.

The prepared nanoparticle powder (0.5 g/40 mL) was placed into 40 mL MES buffer. EDC (38.4 mg/mL) and NHS (38.4 mg/mL) were added to the MES buffer and subjected to 1 h of ultrasonic vibration to activate the amino acids. Adenine (0.5 mg/mL) was added to the resulting solution, which was then transferred to a 50 mL centrifuge tube. The tube was sealed with a sealing film and placed on a shaker at a speed of 140 rpm. The reaction was at room temperature for 24 h to remove bubbles. After centrifugation to discard the supernatant, the sample was washed twice with anhydrous ethanol and dried in an 80 °C vacuum drying oven for 24 h, resulting in powdered samples of γ-Fe_2O_3@SiO_2–NH_2-CMC/MIL-101(Al)–NH_2-Glu-A (γ-Fe_2O_3-CMC/Al-MOF-Glu-A), γ-Fe_2O_3@SiO_2–NH_2-CMC/MIL-101(Al)–NH_2-Asp-A(γ-Fe_2O_3-CMC/Al-MOF-Asp-A), γ-Fe_2O_3@SiO_2–NH_2-CMC/MIL-101(Al)–NH_2-GA-A(γ-Fe_2O_3-CMC/Al-MOF-GA-A), γ-Fe_2O_3@SiO_2–NH_2-AA/MIL-101(Al)–NH_2-Glu-A (γ-Fe_2O_3-AA/Al-MOF-Glu-A), γ-Fe_2O_3@SiO_2–NH_2-AA/MIL-101(Al)–NH_2-Asp-A (γ-Fe_2O_3-AA/Al-MOF-Asp-A) and γ-Fe_2O_3@SiO_2–NH_2-AA/MIL-101(Al)–NH_2-GA-A (γ-Fe_2O_3-AA/Al-MOF-GA-A).

2.3 Jasminaldehyde Condensation Reaction

The Jasminaldehyde condensation reactions between benzaldehyde and 1-heptanal were conducted using the above 6 particles as catalysts. The catalyst particles were subjected to overnight vacuum drying at 110 °C to remove coordinated water to obtain the activated catalyst [21]. Ethanol was used as a solvent to enhance the yield of jasminealdehyde [22]. A three-necked flask equipped with a reflux condenser, magnetic stirrer, and drip funnel was employed. Into this flask, 5.19 mL (0.05 mol) of

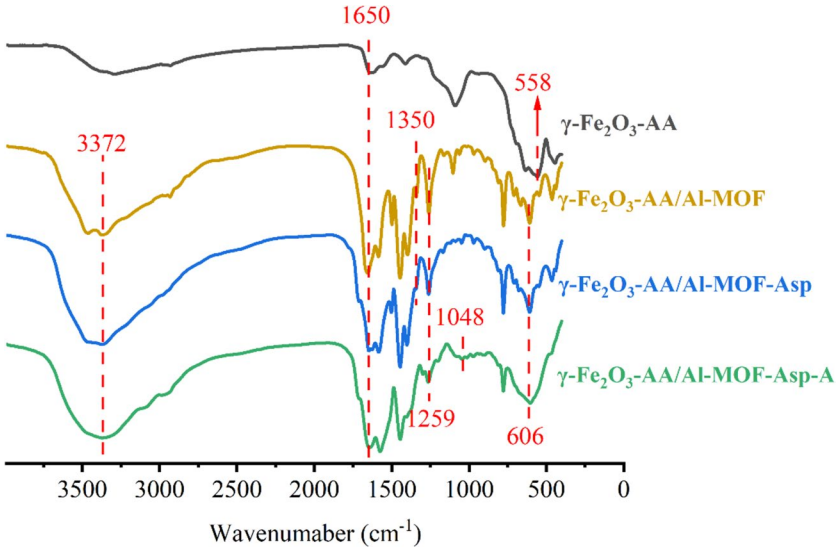

Fig. 2 FTIR spectra: as-prepared γ-Fe_2O_3-AA (black); γ-Fe_2O_3-AA/Al-MOF (yellow); γ-Fe_2O_3-AA/Al-MOF-Asp (blue); γ-Fe_2O_3-AA/Al-MOF-Asp-A (green) (Color figure online)

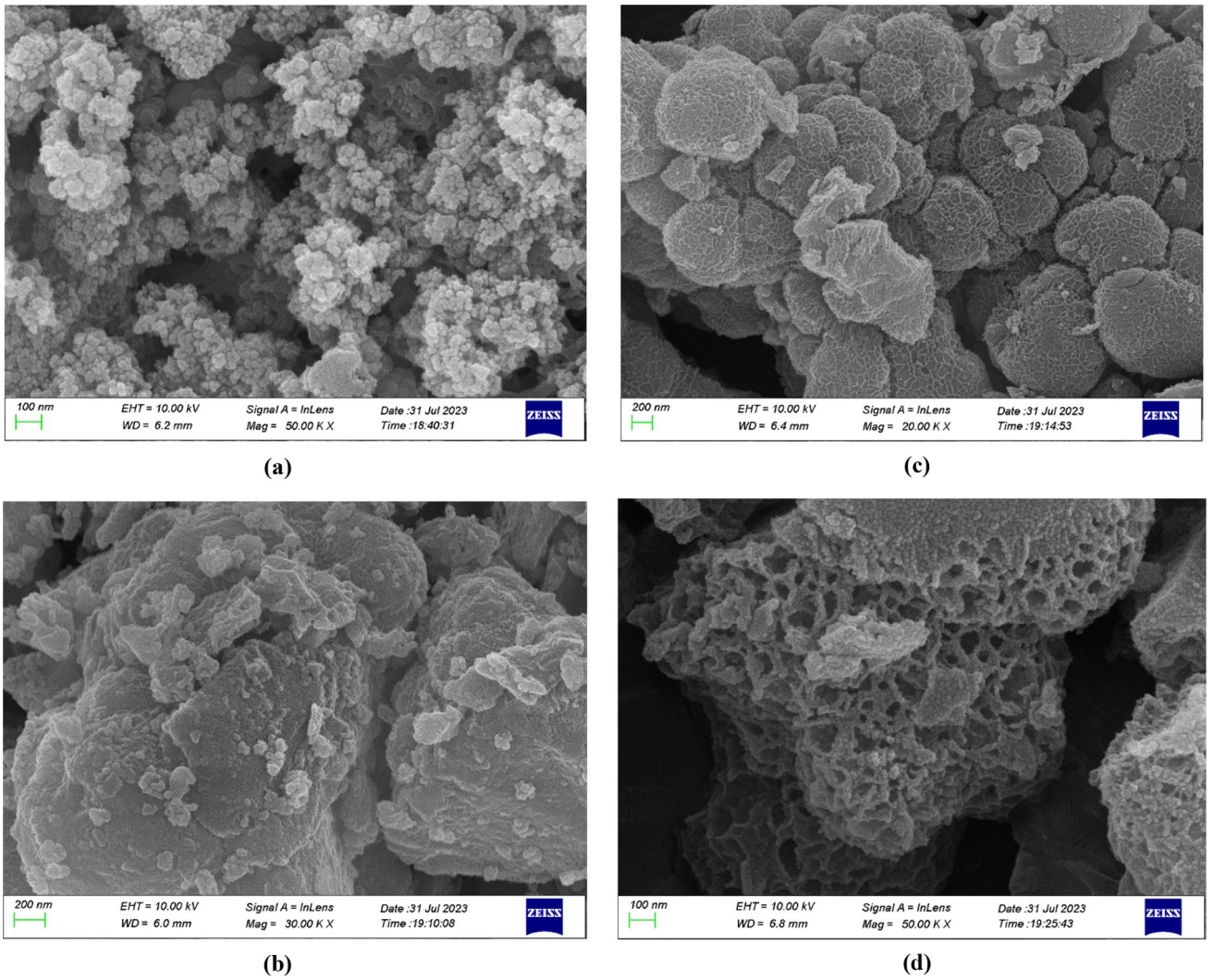

Fig. 3 SEM data: **a** γ-Fe_2O_3@SiO_2–NH_2-AA; **b** γ-Fe_2O_3@SiO_2–NH_2-AA/Al-MOF; **c** γ-Fe_2O_3@SiO_2–NH_2-AA/Al-MOF-Asp-A; **d** γ-Fe_2O_3@SiO_2–NH_2-CMC/Al-MOF-Asp-A samples

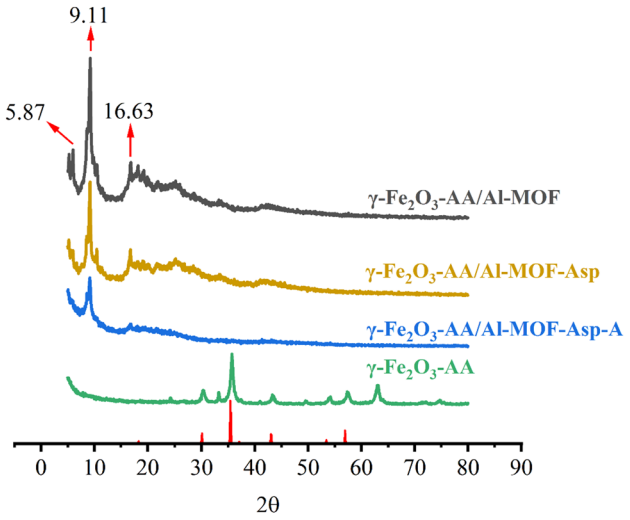

Fig. 4 XRD data: γ-Fe_2O_3-AA/Al-MOF (black); γ-Fe_2O_3-AA/Al-MOF-Asp (yellow); γ-Fe_2O_3-AA/Al-MOF-Asp-A (blue); γ-Fe_2O_3-AA (green); the standard diffraction spectrum of γ-Fe_2O_3 (red) (Color figure online)

benzaldehyde and 15 mL of an ethanol solution containing 0.05 g of catalyst were added. Subsequently, 10 mL of an ethanol solution containing 1.69 mL (0.0125 mol) of 1-heptanal was slowly dripped into the flask using a constant pressure drip funnel. The reaction was carried out in an oil bath at 80 °C for 4 h. After centrifugation and dilution by a factor of 100, the products were analyzed using GC-MS.

3 Results and Discussion

3.1 FTIR Spectra Analysis

A series of products were obtained by PSM of MPNs/MOFs. Subsequent catalytic experiments revealed that the γ-Fe_2O_3-AA/Al-MOF-Asp-A exhibited the best catalytic performance. Therefore, this sample was selected for in-depth characterization and analysis. IR was employed for the characterization of the particles obtained. As shown in Fig. 2, the Fe–O bond in γ-Fe_2O_3 was observed at 558 cm^{-1} [23]. The bands associated with Al-O are observed at 606 cm^{-1}, suggesting the coordination between Al and O atoms [24]. Bands at 1,259 and 1,350 cm^{-1} were indicative of the stretching vibrations of the C–N bond in the benzene ring, while the band at 1,650 cm^{-1} represented the C=O bond. The symmetric stretching vibration peak of the NH2 group on the benzene ring was observed at 3,372 cm^{-1}, indicating the successful modification of MIL-101(Al)–NH_2 on the surface of the nanomaterial [25]. The peak at 1,048 cm^{-1} corresponded to the stretching vibration of the C–N group, which was similar to the signal of the adenine in reference, providing evidence that adenine was present in the material [26].

3.2 SEM Data Analysis

SEM images for the γ-Fe_2O_3-AA, γ-Fe_2O_3-AA/Al-MOF, γ-Fe_2O_3-AA/Al-MOF-Asp-A and γ-Fe_2O_3-CMC/Al-MOF-Asp-A samples were shown in Fig. 3a–d. As shown in Fig. 3a, γ-Fe_2O_3-AA was observed to be dispersed in a regular spherical shape. Small particle sizes in the MNPs/MOFs samples was evident, with almost all particle sizes being less than 1 μm. In Fig. 3c, a groove pattern on the particle surface was observed compared to Fig. 3b, indicating successful PSM modification. In Fig. 3d, a porous structure was observed, which provides an abundance of active sites for interacting with reactants, thereby enhancing the rate of catalytic reactions.

3.3 XRD Analysis

Figure 4 depicts the XRD pattern of MNPs/MOFs materials. The XRD pattern of γ-Fe_2O_3-AA was similar to the standard diffraction spectra as reported in Ref. [27]. The main peaks of MIL-101(Al) could be identified within the 2θ range of 5.87, 9.11, 16.63, and 18.20, consistent with the findings reported in Ref. [28]. This confirmed the successful synthesis of MIL-101(Al) and indicated that the MOF framework had remained intact during the modification process.

3.4 XPS Analysis

As shown in Fig. 5a, the low-resolution XPS survey spectra of γ-Fe_2O_3-AA, γ-Fe_2O_3-AA/Al-MOF, and γ-Fe_2O_3-AA/Al-MOF-Asp-A samples, all of which were semi-quantitative. The XPS spectrum of C1s for γ-Fe_2O_3-AA/Al-MOF (Fig. 5c) showed two peaks at 284.8 and 288.8 eV, corresponding to carboxyl and phenyl signals [29]. The presence of the Al2p peak confirmed the successful synthesis of MIL-101(Al). In accordance with Table 1 and in conjunction with the C1s spectra (Fig. 5b and d), the C=O ratios were found to increase to 18.46%, 26.05%, and 33.03% with the progression of the modification steps. As shown in Fig. 5g, the peaks at 399.8 eV are attributed to the single bond NH2.

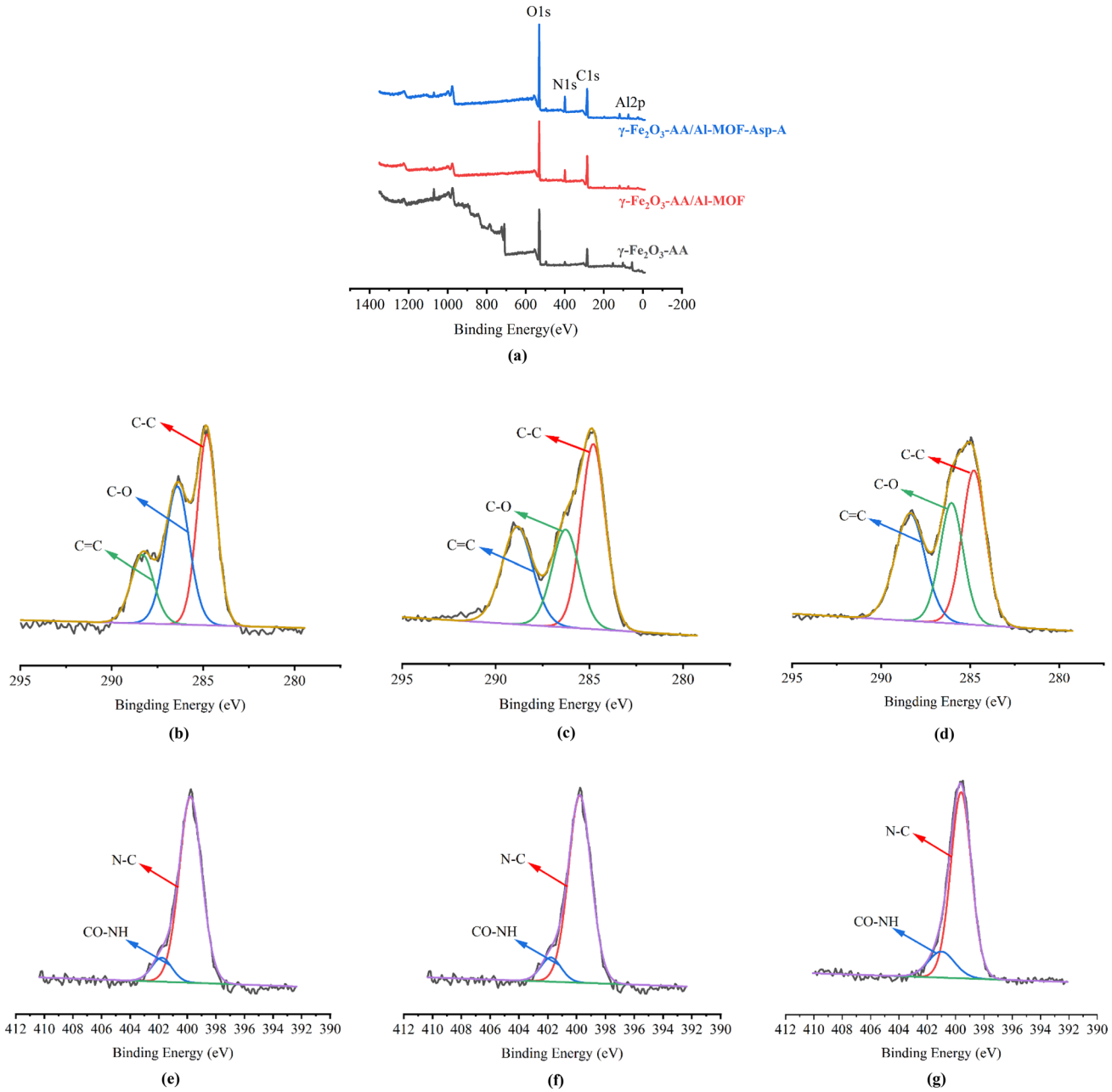

Fig. 5 **a** XPS wide scan spectra of γ-Fe_2O_3-AA, γ-Fe_2O_3-AA/Al-MOF and γ-Fe_2O_3-AA/Al-MOF-Asp-A; **b** high-resolution C1s spectrum of γ-Fe_2O_3-AA; **c** high-resolution C1s spectrum of γ-Fe_2O_3-AA/Al-MOF; **d** high-resolution C1s spectrum of γ-Fe_2O_3-AA/Al-MOF-Asp-A; **e** high-resolution N1s spectrum of γ-Fe_2O_3-AA; **f** high-resolution N1s spectrum of γ-Fe_2O_3-AA/Al-MOF; **g** high-resolution N1s spectrum of γ-Fe_2O_3-AA/Al-MOF-Asp-A

The appearance of a peak at a binding energy of 401.08 eV, corresponding to the CO-NH bond, suggests the formation of amide bonds [30]. Furthermore, the combination of Table 1 with the N1s spectra (Fig. 5e and g) indicated that the CO-NH content increased upon introducing aspartic acid and adenine, signifying successful modification.

3.5 Jasminealdehyde Condensation Results

As depicted in Fig. 6, the retention time of diluted jasminealdehyde was 13.48 min. A comparative control experiment involving six particle types showed that the highest catalytic

Table 1 Binding energy and elemental ratio of each step of the modification process

Samples	Binding energy (eV)		At%
γ-Fe_2O_3-AA	C–C	284.8	43.02
	C–O	286.417	38.52
	C=O	288.326	18.46
	N–C	399.95	72.28
	CO–NH	401.46	27.72
γ-Fe_2O_3-AA/Al-MOF	C–C	284.8	52.13
	C–O	286.188	21.02
	C=O	288.653	26.05↑
	N–C	399.78	89.68
	CO–NH	401.78	10.32
γ-Fe_2O_3-AA/Al-MOF-Asp-A	C–C	284.8	37.91
	C–O	286.054	29.07
	C=O	288.38	33.03↑
	N–C	399.614	84.80
	CO–NH	400.998	15.20↑

activity was exhibited by γ-Fe_2O_3-AA/Al-MOF-Asp-A, with a concentration of jasminealdehyde reaching 1.031 ppm.

To further investigate the influence of catalyst structure on catalytic performance, a comparative analysis was conducted under different conditions, as shown in Fig. 7: (a) without catalyst, (b) γ-Fe_2O_3-AA, (c) γ-Fe_2O_3-AA/Al-MOF, and (d) γ-Fe_2O_3-AA/Al-MOF-Asp-A. The results indicated that significant catalytic effects were observed for γ-Fe_2O_3-AA. The catalytic efficiency of γ-Fe_2O_3-AA/Al-MOF surpasses that of γ-Fe_2O_3-AA, potentially owing to the synergistic catalytic effect facilitated by the core-shell structure. Furthermore, the catalytic performance of γ-Fe_2O_3-AA/Al-MOF-Asp-A particles was further enhanced by employing the PSM technique to introduce amino groups.

Compared to the traditional homogeneous catalyst KOH, as shown in Fig. 8, a solution analysis was conducted immediately after the catalytic reaction and again after 24 h. The results revealed that the concentration of the product catalyzed by the γ-Fe_2O_3-AA/Al-MOF-Asp-A catalyst increased from 1.031 to 1.844, whereas the concentration of the product catalyzed by the KOH catalyst increased from 0.04 to 2.429. These findings suggested that within a relatively short reaction time, significant advantages were exhibited by the γ-Fe_2O_3-AA/Al-MOF-Asp-A catalyst.

At the same time, γ-Fe_2O_3-AA/Al-MOF-Asp-A is highly stable during the reaction without losing its activity. No structural changes are evident from the XRD pattern of the used catalyst, which is almost identical to the fresh material, as shown in Fig. 9.

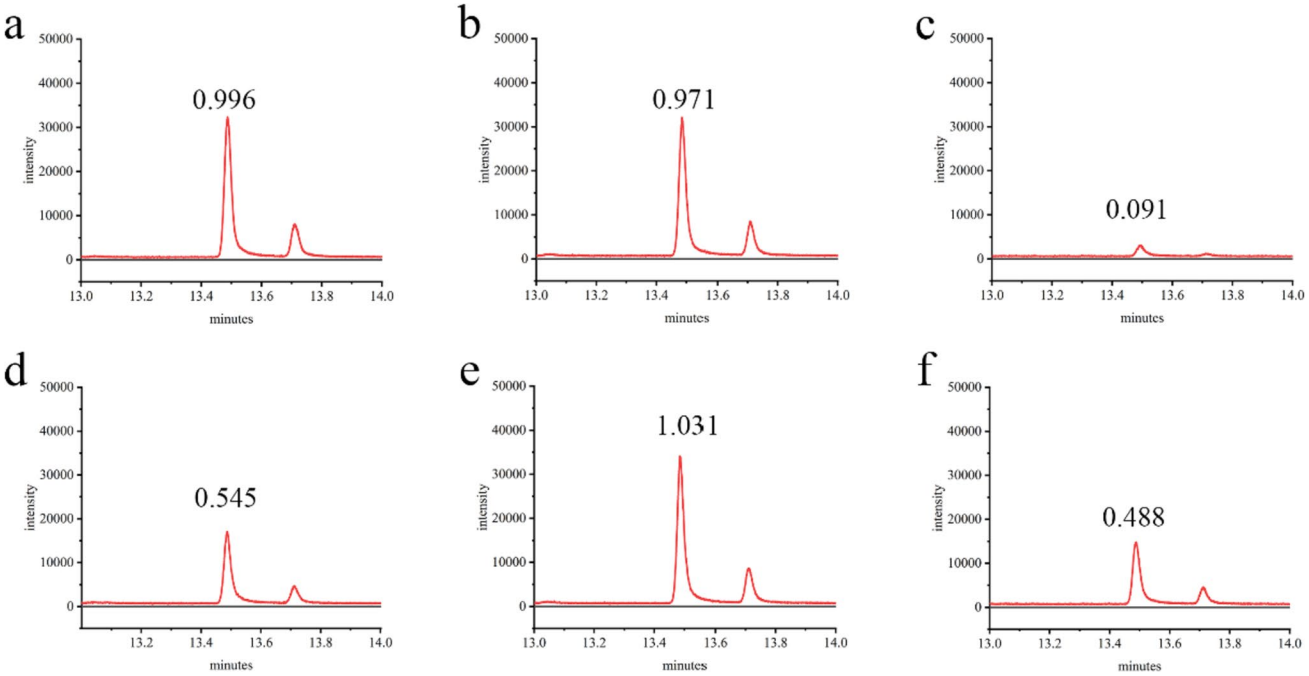

Fig. 6 GC-MS charomatogram of the reaction solution catalyzed of **a** γ-Fe_2O_3-CMC/Al-MOF-Glu-A, **b** γ-Fe_2O_3-CMC/Al-MOF-Asp-A, **c** γ-Fe_2O_3-CMC/Al-MOF-GA-A, **d** γ-Fe_2O_3-AA/Al-MOF-Glu-A, **e** γ-Fe_2O_3-AA/Al-MOF-Asp-A, **f** γ-Fe_2O_3-AA/Al-MOF-GA-A

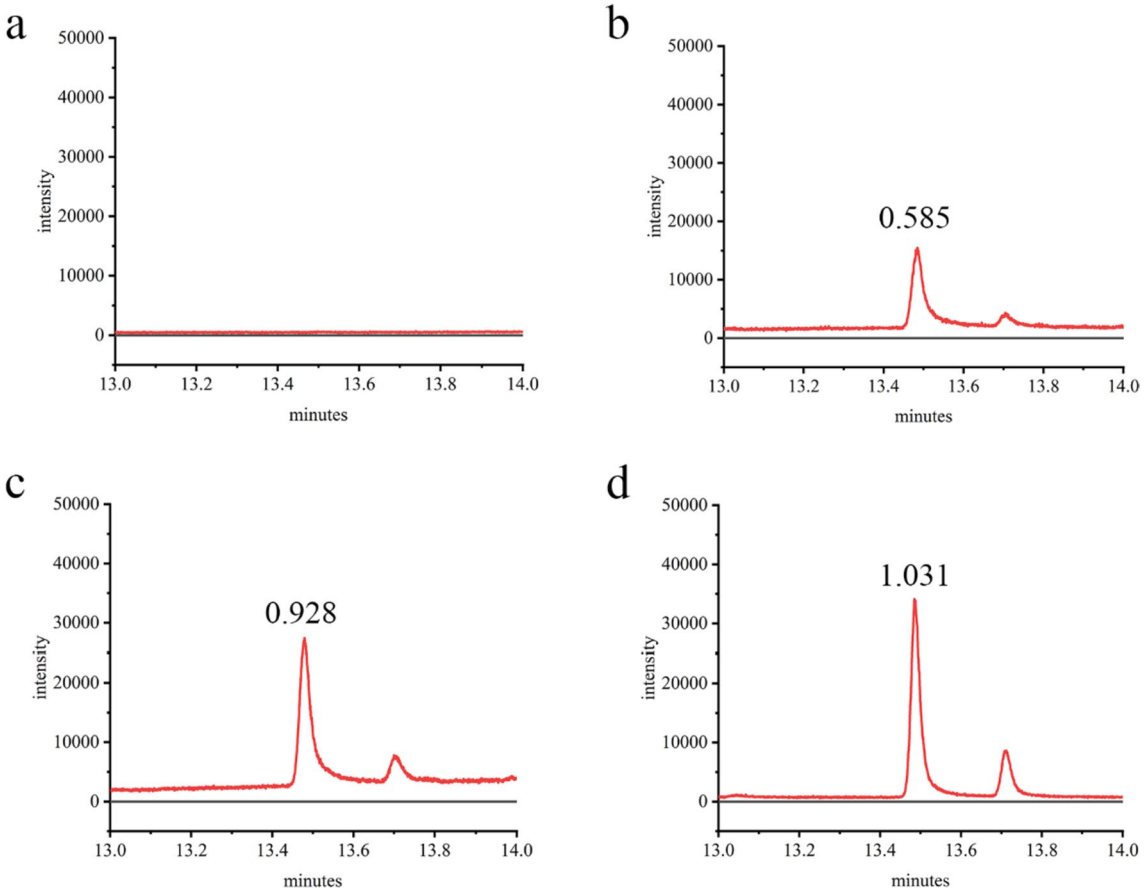

Fig. 7 GC-MS charomatogram of the reaction solution catalyzed of **a** without catalyst, **b** γ-Fe_2O_3-AA, **c** γ-Fe_2O_3-AA/Al-MOF, **d** γ-Fe_2O_3-AA/Al-MOF-Asp-A

4 Conclusions

The MNPs/MOFs core-shell structure was successfully synthesized through one-pot synthesis, and amino groups were introduced using the PSM technique to obtain the γ-Fe_2O_3-CMC/Al-MOF-Glu-A, γ-Fe_2O_3-CMC/Al-MOF-Asp-A, γ-Fe_2O_3-CMC/Al-MOF-GA-A, γ-Fe_2O_3-AA/Al-MOF-Glu-A, γ-Fe_2O_3-AA/Al-MOF-Asp-A, γ-Fe_2O_3-AA/Al-MOF-GA-A powder samples. Characterization of the prepared samples using IR spectroscopy, XRD, and XPS confirmed the successful synthesis and modification of the MNPs/MOFs materials. The XRD measurements of the fresh and used catalysts demonstrate no structural changes, confirming the stability of the catalyst under the current experimental conditions. The typical shapes of MNPs and MNPs/MOFs structures were demonstrated in SEM.

The primary focus of this study was the first-time utilization of MNPs/MOFs core-shell structures for investigating the catalytic performance in the aldol condensation reaction of benzaldehyde and 1-heptanal. Comparative experiments revealed that the core-shell structure formed between MNPs and MOFs significantly enhanced the catalytic yield. Additionally, introducing amino functional groups through PSM technology further improved the catalytic yield. Compared to the traditional homogeneous KOH catalyst, the γ-Fe_2O_3-AA/Al-MOF-Asp-A catalyst offers the advantages of shorter reaction times and being environmentally friendly and recyclable. Our future work will further explore the MNPs/MOFs core-shell structured materials and a detailed comparative study with various traditional homogeneous catalysts and heterogeneous catalysts for the Jasminaldehyde Condensation Reactions.

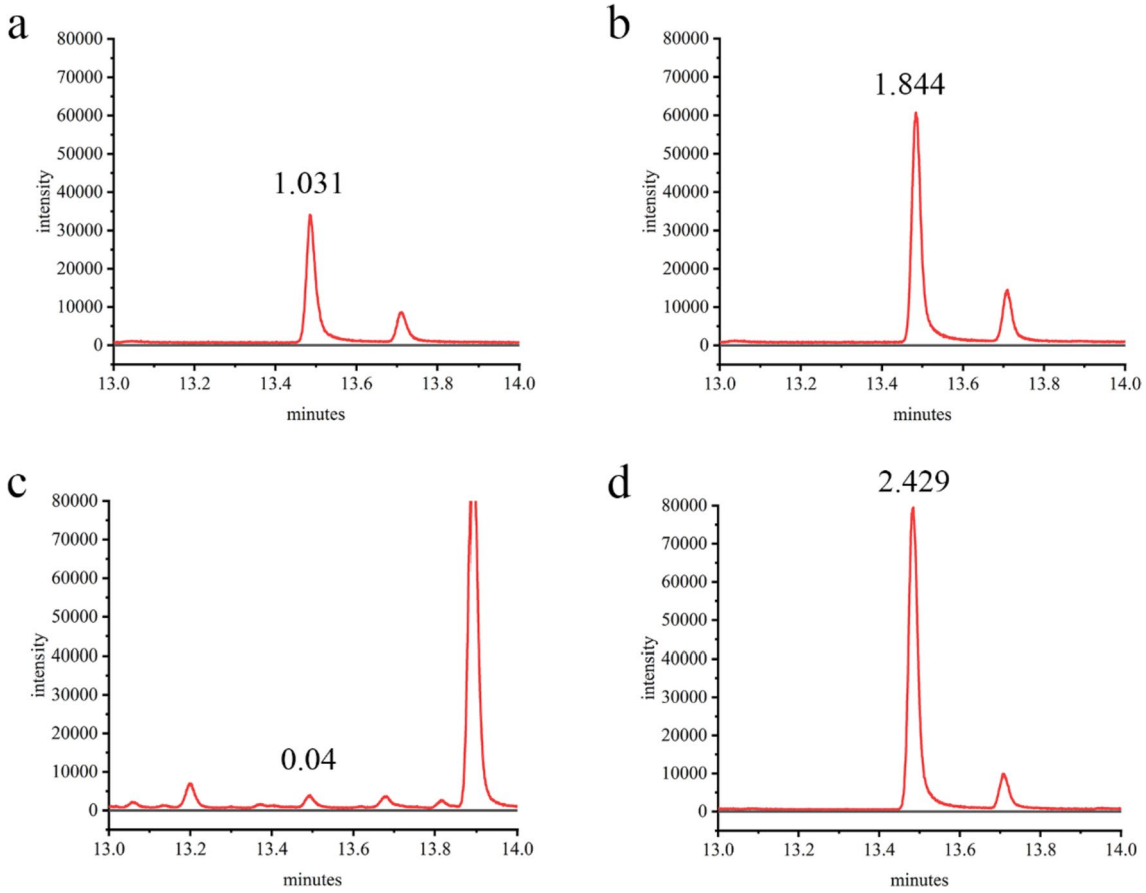

Fig. 8 GC-MS charomatogram of the reaction solution catalyzed of **a** γ-Fe_2O_3-AA/Al-MOF-Asp-A, **b** after 24 h γ-Fe_2O_3-AA/Al-MOF-Asp-A, **c** KOH, **d** After 24 h KOH

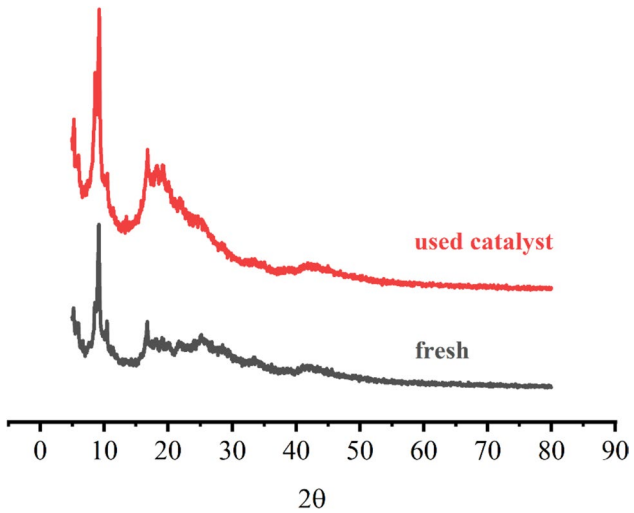

Fig. 9 Powder XRD of γ-Fe_2O_3-AA/Al-MOF-Asp-A, fresh (black); used as catalyst in the Jasminealdehyde condensation (red) (Color figure online)

Author Contributions All the authors (LF, QD, ZZ, RZ, CL, LY) made substantial contribution while preparing the manuscript.

Funding This work was supported by the National Natural Science Foundation of China (Grant Nos. 31372482, 31572492), Tianjin Dairy Cattle (Mutton Sheep) Industrial Technology System Innovation Team Construction Project (ITTCRS2021000), the Veterinary Biotechnology Scientific Research Innovation Team of Tianjin, China (Grant No.TD13-5091), Plan Project of Scientific Research from Tianjin Municipal Education Commission (Grant No. 2019KJ032).

Data Availability The datasets generated during and analysed during the current study are available from the corresponding author on reasonable request.

Declarations

Conflict of interest The authors declare no competing interests.

References

1. N. Wang, Q. Sun, J. Yu, Ultrasmall metal nanoparticles confined within crystalline nanoporous materials: a fascinating class of nanocatalysts. Adv. Mater. **31**(1), 1803966 (2019)
2. L. Niu, G. Zhang, G. Xian, Z. Ren, T. Wei, Q. Li, Y. Zhang, Z. Zou, Tetracycline degradation by persulfate activated with magnetic γ-Fe_2O_3/CeO_2 catalyst: performance, activation mechanism and degradation pathway. Sep. Purif. Technol. **259**, 118156 (2021)
3. F.A. Fadeyev, F.A. Blyakhman, A.P. Safronov, G.Y. Melnikov, A.D. Nikanorova, I.P. Novoselova, G.V. Kurlyandskaya, Biological impact of γ-Fe_2O_3 magnetic nanoparticles obtained by laser target evaporation: focus on magnetic biosensor applications. Biosensors **12**(8), 627 (2022)
4. S. Kamali, E. Yu, B. Bates, J.R. McBride, C.E. Johnson, V. Taufour, P. Stroeve, Magnetic properties of γ-Fe_2O_3 nanoparticles in a porous SiO_2 shell for drug delivery. J. Phys.: Condens. Matter **33**(6), 065301 (2020)
5. H. Ghasempour, K.-Y. Wang, J.A. Powell, F. ZareKarizi, X.-L. Lv, A. Morsali, H.-C. Zhou, Metal-organic frameworks based on multicarboxylate linkers. Coord. Chem. Rev. **426**, 213542 (2021)
6. T. Jia, Y. Gu, F. Li, Progress and potential of metal-organic frameworks (MOFs) for gas storage and separation: a review. J. Environ. Chem. Eng. **10**(5), 108300 (2022)
7. X. Li, K. Chen, R. Guo, Z. Wei, Ionic liquids functionalized MOFs for adsorption. Chem. Rev. **123**(16), 10432–10467 (2023)
8. D.H. Hong, H.S. Shim, J. Ha, H.R. Moon, MOF-on-MOF architectures: applications in separation, catalysis, and sensing. Bull. Korean Chem. Soc. **42**(7), 956–969 (2021)
9. A. Bieniek, A.P. Terzyk, M. Wiśniewski, K. Roszek, P. Kowalczyk, L. Sarkisov, S. Keskin, K. Kaneko, MOF materials as therapeutic agents, drug carriers, imaging agents and biosensors in cancer biomedicine: recent advances and perspectives. Prog. Mater. Sci. **117**, 100743 (2021)
10. H. Liu, L. Chen, J. Ding, Adsorption behavior of magnetic amino-functionalized metal-organic framework for cationic and anionic dyes from aqueous solution. RSC Adv. **6**(54), 48884–48895 (2016)
11. M. Taghizadeh, S. Tahami, Recent developments in MIL-101 metal organic framework for heterogeneous catalysis. Rev. Chem. Eng. **39**(4), 707–728 (2023)
12. M. Gopalan Sibi, D. Verma, J. Kim, Magnetic core–shell nanocatalysts: promising versatile catalysts for organic and photocatalytic reactions. Catal. Rev. **62**(2), 163–311 (2020)
13. F. Ke, L. Wang, J. Zhu, An efficient room temperature core–shell AgPd@MOF catalyst for hydrogen production from formic acid. Nanoscale **7**(18), 8321–8325 (2015)
14. X. Song, Y. He, Z. Cai, X. Li, Y. Sun, H. Liu, Y. Lu, J. Hou, E. Han, Three amino-functionalized alkaline earth metal-organic frameworks as catalysts for knoevenagel condensation. ChemistrySelect **5**(37), 11510–11516 (2020)
15. N. Sudheesh, R.S. Shukla, Investigations on different efficient strategies for the selective synthesis of jasminaldehyde over HRhCO(PPh3)3–hexagonal mesoporous silica and chitosan catalysts. Reaction Kinet. Mech. Catal. **135**(3), 1485–1502 (2022)
16. A. Fan, Acid–base bifunctional magnesium oxide catalyst prepared from a simple hydrogen peroxide treatment for highly selective synthesis of jasminaldehyde. Energy Sour. Part a Recover. Utilization Environ. Eff. **42**(20), 2501–2515 (2020)
17. L. Yang, L. Fu, B. Li, J. Ma, C. Li, T. Jin, W. Gu, L. Yang, L. Fu, B. Li, J. Ma, C. Li, T. Jin, W. Gu, Fluorescence enhancement method for enrofloxacin extraction by core-shell magnetic microspheres. Aust. J. Chem. **73**(11), 1105–1111 (2020)
18. B. Li, M. Qin, X. Liu, J. Gao, Q. Song, L. Yang, Knoevenagel condensation catalyzed by core-shell magnetic microspheres. Acta Scientiarum Naturalium Universitatis Nankaiensis **53**(4), 93–98 (2020)
19. R. Rani, A. Deep, B. Mizaikoff, S. Singh, Enhanced hydrothermal stability of Cu MOF by post synthetic modification with amino acids. Vacuum **164**, 449–457 (2019)
20. C. Feng, S. Qiao, Y. Guo, Y. Xie, L. Zhang, N. Akram, S. Li, J. Wang, Adenine-assisted synthesis of functionalized F–Mn–MOF-74 as an efficient catalyst with enhanced catalytic activity for the cycloaddition of carbon dioxide. Colloids Surfaces A: Physicochem. Eng. Aspects **597**, 124781 (2020)
21. Q. Li, J. Liu, Z. Ren, Z. Wang, F. Mao, H. Wu, R. Zhou, Y. Bu, Catalytic degradation of antibiotic by Co nanoparticles encapsulated in nitrogen-doped nanocarbon derived from Co-MOF for promoted peroxymonosulfate activation. Chem. Eng. J. **429**, 132269 (2022)
22. P.M. Heynderickx, Activity coefficients for liquid organic reactions: towards a better understanding of true kinetics with the synthesis of jasmin aldehyde as showcase. Int. J. Mol. Sci. **20**(15), 3819 (2019)
23. T. Tasheva, R. Harizanova, I. Mihailova, Z. Cherkezova-Zheleva, D. Paneva, M. Nedkova, C. Rüssel, Structure and redox ratio of soda-lime-silica glasses with high iron oxide concentrations. Int. J. Appl. Glass Sci. **14**(3), 445–454 (2023)
24. D. Xie, X. Ge, W. Qin, Y. Zhang, NH2-MIL-53(Al) for simultaneous removal and detection of fluoride anions. Chin. J. Chem. Phys. **34**(2), 227–237 (2021)
25. S. Ahmadipouya, F. Ahmadijokani, H. Molavi, M. Rezakazemi, M. Arjmand, CO_2/CH_4 separation by mixed-matrix membranes holding functionalized NH_2-MIL-101(Al) nanoparticles: effect of amino-silane functionalization. Chem. Eng. Res. Des. **176**, 49–59 (2021)
26. T.T.T. Nguyen, H.T. NguyenL, N.X.D. Mai, H.K.T. Ta, T.L.T. Nguyen, U.-C.N. Le, B.T. Phan, N.N. Doan, T.L.H. Doan, Mild and large-scale synthesis of nanoscale metal-organic framework usedas a potential adenine-based drug nanocarrier. J. Drug DeliverySci. Technol. **61**, 102135 (2021)
27. S. Li, X. Liu, J. Xu, D. Wei, C. Li, R. Zhao, L. Yang, Magnetic solid-phase extraction of norfloxacin by core-shell magnetic nanoparticles. J. Coord. Chem. **75**(7–8), 925–936 (2022)
28. S. Li, T. Lei, F. Jiang, M. Liu, Y. Wang, S. Wang, X. Yang, Tuning the morphology and adsorption capacity of Al-MIL-101 analogues with Fe^{3+} for phosphorus removal from water. J. Colloid Interface Sci. **560**, 321–329 (2020)
29. T.A. Vu, G.H. Le, C.D. Dao, L.Q. Dang, K.T. Nguyen, P.T. Dang, H.T. Tran, Q.T. K, Duong, T.V. Nguyen, G.D. Lee, Isomorphous substitution of Cr by Fe in MIL-101 framework and its application as a novel heterogeneous photo-Fenton catalyst for reactive dye degradation. RSC Adv. **4**(78), 41185–41194 (2014)
30. S. Wang, H. Luo, X. Li, L. Shi, B. Cheng, X. Zhuang, Z. Li, Amino acid-functionalized metal organic framework with excellent proton conductivity for proton exchange membranes. Int. J. Hydrog. Energy **46**(1), 1163–1173 (2021)

Publisher's Note Springer nature remains neutral with regard to jurisdictional claims in published maps and institutional affiliations.

Springer Nature or its licensor (e.g. a society or other partner) holds exclusive rights to this article under a publishing agreement with the author(s) or other rightsholder(s); author self-archiving of the accepted manuscript version of this article is solely governed by the terms of such publishing agreement and applicable law.